energies

MDPI

Article

Optimal Integration of Distribution Network Reconfiguration and Conductor Selection in Power Distribution Systems via MILP

Luis A. Gallego Pareja [1], Jesús M. López-Lezama [2,*] and Oscar Gómez Carmona [3]

[1] Department of Electrical Engineering, State University of Londrina (UEL), Londrina 86057-970, PR, Brazil; luispareja@uel.br
[2] Research Group in Efficient Energy Management (GIMEL), Departamento de Ingeniería Eléctrica, Universidad de Antioquia, Calle 67 No. 53-108, Medellín 050010, Colombia
[3] Facultad de Tecnología, Universidad Tecnológica de Pereira, Cr 27 No 10-02, Pereira 660003, Colombia; jr@utp.edu.co
* Correspondence: jmaria.lopez@udea.edu.co

Abstract: Power distribution systems (PDS) comprise essential electrical components and infrastructure that facilitate the delivery of electrical energy from a power transmission system to end users. Typically, the topology of distribution systems is radial, so that power goes from the substations to end users through main lines or feeders. However, the expansion of new feeders to accommodate new users and ever-growing energy demand have led to higher energy losses and deterioration of the voltage profile. To address these challenges, several solutions have been proposed, including the selection of optimal conductors, allocation of voltage regulators, utilization of capacitor banks, implementation of distributed generation, and optimal reconfiguration. Although reconfiguring the network is the most cost-effective approach, this solution might not be sufficient to completely minimize technical losses and improve system performance. This paper presents a novel approach that combines optimal distribution network reconfiguration (ODNR) with optimal conductor selection (OCS) to minimize power losses and enhance the voltage profiles of PDS. The key contribution lies in the integration of the ODNR and OCS into a single MILP problem, ensuring the attainment of globally optimal solutions. The proposed model was tested with benchmark 33-, 69-, and 85-bus test systems. The results allowed us to conclude that the combined effect of ODNR and OCS presents better results than when any of these approaches are applied either separately or sequentially.

Keywords: power distribution systems; optimal reconfiguration; optimal conductors selection; mixed-integer linear model

Citation: Gallego Pareja, L.A.; López-Lezama, J.M.; Gómez Carmona, O. Optimal Integration of Distribution Network Reconfiguration and Conductor Selection in Power Distribution Systems via MILP. *Energies* **2023**, *16*, 6998. https://doi.org/10.3390/en16196998

Academic Editor: Akhtar Kalam

Received: 24 August 2023
Revised: 21 September 2023
Accepted: 6 October 2023
Published: 8 October 2023

1. Introduction

In today's electric power industry, the efficient and reliable operation of PDS has become a predominant concern. The increasing demand for electricity, coupled with the integration of renewable energy sources and the advent of smart grid technologies, increases the complexity of PDS planning and operation. To address the challenges posed by this complexity, researchers are turning their attention to advanced optimization techniques. This paper explores a critical aspect of PDS optimization—the seamless integration of ODNR and OCS through the application of mixed-integer linear programming (MILP). By harnessing the potential of MILP, this study aims to improve voltage regulation and mitigating power losses in PDS.

OCS plays an important role in ensuring the reliable and efficient operation of PDS. Conductors distribute electrical energy from distribution substations to final customers through principal feeders and laterals. With the increasing demand for electricity and the integration of renewable energy sources, the need for OCS becomes crucial. The choice of

conductors impacts various aspects of PDS, including power losses, voltage regulation, and overall system reliability. An inefficient conductor selection may lead to elevated energy losses, voltage drop issues, and increased operational costs. Conversely, OCS results in reduced power losses, improved voltage profiles, and enhanced system longevity.

The primary objective of OCS is to replace the current conductors in a feeder with different types of conductors. This replacement aims to decrease active power losses, enhance the capacity of circuits, and raise voltage levels. The OCS is a highly complex problem, which can be represented as a mixed integer nonlinear programming (MINLP) problem. Researchers have employed exact techniques as well as heuristic and metaheuristic approaches to tackle this optimization problem.

Heuristics are search techniques that prioritize speed over optimality and are often used when dealing with complex or computationally challenging tasks [1,2]. Although they may not always guarantee the global optimal solution, heuristic and metaheuristic techniques are valuable tools in non-convex optimization and decision-making processes. In the context of OCS, researchers have proposed various heuristic-based approaches. For instance, in [3] the authors presented a methodology combining an economically driven current density-based approach with a heuristic approach for optimizing the conductor selection in radial PDS. In this case, a branching feeder approach without uniform load distribution was used to approximate the real conditions of most PDS. Another study [4] proposed a branch-wise minimization technique for selecting the optimum size of conductors in radial PDS. The conductors selected by the proposed approach maximized the total savings in costs, including conductor material and energy losses while maintaining acceptable voltage profiles. In [5], the authors considered financial and engineering factors as key aspects of OCS. In this case, operating and capital costs were considered bearing in mind a set of conductors with the most economic cost characteristics and enough thermal capacity to meet high-demand scenarios. In [6], a general methodology for optimal conductor size selection in PDS was presented aiming to minimize the total conductor and power loss cost. The model includes diversity in load peaks, load factors, cost of power, load increments, and cost of energy in the decision-making process.

A comparative study between an analytical method and a genetic algorithm (GA) to solve the OCS problem was carried out in [7]. In this case, the analytical approach was based on consecutive load flows. A two-phase methodology employing the branch-wise minimization technique was proposed in [8] to solve OCS in radial PDS. In [9], the authors presented an analytical approach comparing power flow results for distinct ACSR conductors. It is important to note that heuristic optimization techniques cannot ensure a solution that is globally optimal; instead, they offer a proper estimation. These methods may encounter locally optimal solutions and can be computationally intensive, especially when dealing with large-scale problems involving numerous variables.

Metaheuristics have also gained significant popularity in solving the OCS problem. These approaches are inspired by natural and social phenomena such as evolutionary processes or swarm intelligence. In evolutionary and genetic algorithms, a population of potential solutions is evolved over generations through processes such as selection, crossover, and mutation. OCS has been solved through genetic algorithms (GAs) [7,10], adaptive genetic algorithm (AGA) [11], evolutionary strategies (ES) [12], differential evolution algorithm (DEA) [13], and discrete genetic algorithm (DGA) [14].

Particle swarm optimization (PSO) is a metaheuristic approach inspired by the social behavior of some organisms such as schools of fish and flocks of birds. The OCS has also been solved through PSO [15,16], selective particle swarm optimization (SPSO) [17], discrete particle swarm optimization (DPSO) [18] and salp swarm optimization (SSO) [19].

In harmony search algorithms (HSAs), a set of candidate solutions, labeled as harmonies, represent potential solutions to the optimization problem. The OCS problem was solved using HSA with a differential operator (HSDE) in [20]. Other metaheuristic approaches adapted for solving the OCS problem in PDS include crow search algorithm

(CSA) [21], sine–cosine optimization algorithm (SCA) [22], Tabu search (TS) [23] and Newton's metaheuristic algorithm (NMA) [24].

Even though metaheuristic approaches are suitable for solving complex optimization problems, they may not consistently reach the absolute global solution. Moreover, they often need significant adjustments to achieve acceptable results, and this can consume a significant amount of time and necessitate specialized knowledge.

Exact techniques have been employed to a lesser extent in solving the OCS problem. These techniques ensure convergence by utilizing existing optimization software. In the literature review, few research studies were found where exact techniques were employed for solving the OCS. Among these papers, one of them utilized a linear model. In the study conducted by the authors of [25], a MILP problem was proposed, accompanied by a heuristic approach to derive the Pareto front for the problem of optimal conductor sizing. The authors of [26] presented a MINLP model for the OCS problem, which was resolved utilizing the general algebraic modeling system (GAMS) with the aid of the DICOPT optimization solver. In [27], the authors developed an exact nonlinear model for the conductor selection, utilizing available MINLP solvers. Lastly, the authors of [28] proposed a MINLP formulation for OCS in DC radial PDS.

Planning strategies, such as reconfiguration, conductor selection, capacitor placement, and DG placement, are commonly studied separately. Nonetheless, the combination of two or more of these techniques may lead to a better-planned system. The problem of OCS has been integrated with capacitor placement in numerous research investigations, where the researchers employed metaheuristic approaches to direct the exploration procedure. However, from the review of existing literature, OCS has not been discussed in simultaneity with optimal distribution network reconfiguration (ODNR) so far.

ODNR is carried out by altering the topology of the distribution network, considering objectives such as minimizing power losses, improving voltage profile, and enhancing network reliability. ODNR is executed by opening and closing tie and sectionalizing switches, respectively, [29]. Due to the nature of its decision variables and constraints, ODNR can be classified as a mixed-integer nonlinear (MINL) optimization problem, usually requiring the aid of metaheuristic techniques for its solution. Early reconfiguration studies were limited to small-sized PDS [30]. This is due to the fact that ODNR is a complex optimization problem that involves both discrete and continuous decision variables. Furthermore, ensuring a radial topology is not a trivial task [31]. Basically, two optimization paradigms are applied to solve the ODNR problem: mathematical programming methods and metaheuristic techniques.

In [32], the authors proposed an optimal power flow and sensitivity analysis approach to solve the ODNR problem, aiming to minimize active power losses. A heuristic approach was implemented by closing all sectionalizing switches and then determining the ones to be reopened to avoid loops in the system. PSO was implemented in [33–35] to tackle the ODNR problem to minimize power losses. In [36–41], several variants of GAs were tested to solve the ODNR problem. In this case, network topologies were represented by binary strings representing the open or closed states of the switches. Then, other topologies were created through both the selection and mutation stages of the GA. In each iteration, the radial condition of the new solutions was verified. In [42,43], the authors solved the ODNR problem through firefly optimization (FO). In this case, ref. [42] considered both ODNR and optimal DG sizing, whereas [43] did not optimize the size of DG in the network; nonetheless, a search space-reducing strategy is implemented to accelerate convergence. The authors of [44,45] proposed an HSA to solve the ODNR problem for minimizing power losses. The proposed approach in [45] also includes island detection to enforce radiality. The TS metaheuristic technique was also applied in [46,47] to solve the ODNR problem. In [46], the authors considered a mutation mechanism to escape from local optima, whereas [47] implemented a random mechanism with the same purpose.

In [48], the authors developed a hybrid data-driven and model-based distribution network reconfiguration approach. A hierarchical network recovery process was imple-

mented to speed up the process. ODNR can also be implemented to enhance network reliability. In [49], a column and constraint generation algorithm was proposed to minimize load curtailments under failures of lines or generators. In [50], the authors presented a reinforcement learning approach that resorts to ODNR to minimize load curtailment. The distribution system is modeled as a graph and the ODNR is determined by searching for a spanning tree that presents minimum curtailed power.

Multi-objective approaches have also been implemented in the reconfiguration problem. In [51], the authors developed an NSGAII approach that minimizes both active power losses and voltage offset of distribution networks. In [52], a multi-objective PSO was proposed to minimize total active power losses and maximize the absorption of renewable DG through a time-varying ODNR. In [53], the authors carried out ODNR with four objectives, namely, power loss minimization, voltage profile improvement, network reliability improvement, and operation costs minimization. The literature on metaheuristics applied to solve the ODNR is wide and varied, and a comparative study on this subject can be consulted in [54].

Apart from heuristic and metaheuristic techniques, some mathematical approaches have also been explored to tackle the ODNR problem. In [55], the authors presented a mathematical model of path connectivity for ODNR. This model is based on the closed-loop design and open-loop operation of DPS. In [56], the authors solve the ODNR problem bearing in mind the power loss minimization and the improvement of reliability. The epsilon-constrained method is used, and the proposed mathematical model is then solved through the algebraic modeling systems (GAMS) software. In [57], a mixed-integer two-stage formulation is proposed to solve the ODNR for minimizing power losses. The master–slave methodology was modeled through a decomposition algorithm in AMPL and subsequently resolved with the utilization of CPLEX.

In DPSs that feature fairly loaded feeders and poor voltage profiles, ODNR alone may not be enough to minimize power losses. Furthermore, as the size and type of conductor for each feeder segment are chosen based on the current carrying capacity of the feeder configuration, and ODNR affects the system operational conditions, simultaneous ODNR and OCS could lead to low-cost planning of PDS; nonetheless, this approach has not been reported in the specialized literature Therefore, the main contribution of this paper lies in the simultaneous formulation and resolution of ODNR and OCS in PDS; furthermore, the proposed MILP model guarantees the globally optimal solution. Finally, the proposed model is suitable for applications in real-size distribution systems through commercially available software. Although a specific table of conductors was used for the test and results, the model allows the use of any set of candidate conductors for OCS.

The remainder of this paper is structured as follows: In Section 5, a nonlinear mathematical framework is presented to tackle the combined ODNR and OCS. Elaboration on the linearization procedures employed to transform the initial model into a MILP problem is provided in Section 3. The outcomes of implementing the suggested model on various benchmark test systems are shown in Section 4. Lastly, the conclusions drawn from this study are presented in Section 5.

2. Nonlinear Mathematical Model for the Integrated ODNR and OCS

This section presents the initial nonlinear mathematical model for the integration of ODNR and OCS in PDS. This initial model presents integer and continuous variables; nonetheless, there are some variable multiplications that will be later linearized to recast this initial approach into a MILP model.

In [58], starting from a nonlinear model of the power flow in PDS, the authors propose and validate a linear model of it. In this case, a comparative analysis was conducted between a linear version of the power flow and the nonlinear power flow applied to seven distribution test systems. The results revealed that the linear model had a maximum error of 0.16%, demonstrating that this model accurately solves the load flow. The linear model proposed by the authors in [58] is then adapted to solve the ODNR problem.

On the other hand, in [59] a MILP for the OCS and the optimal capacitor placement in PDS is presented by the same authors. In this case, the linear power flow proposed in [58] is used for the optimal conductor selection. The models presented by the authors in [58,59] are modified and adapted in this paper to have a single MILP model that solves the OCS and ODNR problems jointly, separately or sequentially. The mathematical optimization model implemented in this paper is designed for radial EDNs and considers the following hypotheses: (i) the EDN is represented by a monophasic equivalent; (ii) Loads are represented as constant power injections; (iii) only an electric source (substation) is considered; (iv) active and reactive power losses in distribution lines are concentrated in their sending bus; and (v) the capacitive reactance of distribution lines is neglected.

2.1. Objective Function

The proposed objective function is formulated through Equation (1), comprising two components. The initial component aims to minimize the cost of annual energy loss. Here, K_p, K_e, T, and LF correspondingly stand for the annual demand cost averaged over time, energy expenses, the annual time in hours, and the system loss factor. Ω_l signifies the collection of branches, whereas Ω_c denotes the collection of available conductor types. It is important to note that the nonlinearity in the first term of the objective function arises from the multiplication of decision variables $W_{ij,c}$ and I_{ij}^{sqr}, representing the selected conductor type c for installation in branch ij (a binary variable) and the square of the current magnitude in the same branch. The linearization of this product is detailed in a subsequent section of this paper. Furthermore, L_{ij} signifies the length of the conductor linked with branch ij, and R_c represents the resistance of conductor type c (measured in kΩ/km).

The second term of the objective function aims at minimizing the annual conductor selection costs. In this case, CRF is the capital recovery factor related to the selection of a new conductor, and C_c is the conductor cost of conductor type c.

$$\text{Minimize } f = \left[K_p + (K_e \cdot T \cdot LF)\right] \sum_{\forall ij \in \Omega_l} \sum_{\forall c \in \Omega_c} L_{ij} \cdot R_c \cdot W_{ij,c} \cdot I_{ij}^{sqr} + CRF \sum_{\forall ij \in \Omega_l} \sum_{\forall c \in \Omega_c} L_{ij} \cdot C_c \cdot W_{ij,c} \quad (1)$$

2.2. Power Balance Constraints

Equation (2) expresses the balance of active power within every bus of the PDS. P_{ki} and P_{ij} denote the active power transmission in branches ki and ij, respectively. P_i^s signifies the active power provided from the substation at bus i. P_i^d represents the active power requirement at bus i. Lastly, Ω_b denotes the collection of buses within the PDS.

$$\sum_{\forall ki \in \Omega_l} P_{ki} - \sum_{\forall ij \in \Omega_l} P_{ij} - \sum_{\forall ij \in \Omega_l} \sum_{\forall c \in \Omega_c} \left(L_{ij} \cdot R_c \cdot W_{ij,c} \cdot I_{ij}^{sqr}\right) + P_i^s = P_i^d; \ \ \forall i \in \Omega_b \quad (2)$$

Equation (3) signifies the equilibrium of reactive power within each bus of the PDS. Q_{ki} and Q_{ij} represent the reactive power flow in branches ki and ij, respectively. $X_{ij,c}$ denotes the inductive reactance of branch ij related to conductor type c. Q_i^s is the reactive power provided from the substation at bus i. Q_i^d stands for the reactive power demand at bus i.

$$\sum_{\forall ki \in \Omega_l} Q_{ki} - \sum_{\forall ij \in \Omega_l} Q_{ij} - \sum_{\forall ij \in \Omega_l} \sum_{\forall c \in \Omega_c} \left(L_{ij} \cdot X_c \cdot W_{ij,c} \cdot I_{ij}^{sqr}\right) + Q_i^s = Q_i^d; \ \ \forall i \in \Omega_b \quad (3)$$

Note that Equations (2) and (3) are nonlinear due to the multiplication of the decision variables $W_{ij,c}$ and I_{ij}^{sqr}. The linearization of this product is presented in a later section of this paper.

2.3. Voltage Drop in the Branches of the PDS

Equation (4) illustrates the voltage reduction within each branch of the PDS. In this context, voltage magnitudes are given in relation to the electrical characteristics of the branches and their load flow. Variables V_i^{sqr} and V_j^{sqr} represent the squared voltage magnitudes at buses i and j, respectively. $Z_c^2 = R_c^2 + X_c^2$ is the square of the impedance of conductor type c, and b_{ij} is a continuous auxiliary variable used to enforce Equation (4); it may take different values depending on whether the circuit ij is open or closed.

$$V_i^{sqr} - V_j^{sqr} = 2 \cdot L_{ij} \sum_{\forall c \in \Omega_c} \left(R_c \cdot W_{ij,c} \cdot P_{ij} + X_c \cdot W_{ij,c} \cdot Q_{ij} \right) + L_{ij}^2 \cdot Z_c^2 \cdot W_{ij,c} \cdot I_{ij}^{sqr} + b_{ij};\ \forall ij \in \Omega_l \tag{4}$$

2.4. Voltage and Current Limits

Equation (5) indicates the voltage magnitude limit at bus i. Note that $\overline{V}_i^2$ and $\underline{V}_i^2$ represent the upper and lower squared voltage magnitude limits at bus i, respectively.

$$\underline{V}_i^2 \leq V_i^{sqr} \leq \overline{V}_i^2;\ \ \forall\, i \in \Omega_b \tag{5}$$

Equation (6) represents the current magnitude limit of the branch ij, where $\overline{I}_{ij,c}^2$ is the upper limit of the square current in branch ij of the conductor type c; y_{ij}^+ and y_{ij}^- are binary variables related to the power flow direction of the branch ij and are used in the ODNR problem. If any one of these variables is equal to one, the switch in the respective branch is closed; if both variables are zero, the circuit is open. $W_{ij,c}$ is used to select the conductor type.

$$0 \leq I_{ij}^{sqr} \leq \sum_{c \in \Omega_c} \left(\overline{I}_{ij,c}^2 \cdot W_{ij,c} \right) \cdot \left(y_{ij}^+ + y_{ij}^- \right);\ \ \forall\, ij \in \Omega_l \tag{6}$$

2.5. Apparent Power Constraint

The left side of Equation (7) is the linearization of V_j^{sqr} times I_{ij}^{sqr}; furthermore, the right side of this equation is the linearization of P_{ij}^2 plus Q_{ij}^2 which are carried out as indicated in [58].

$$\left(\underline{V}^2 + \frac{1}{2}\Delta V \right) \cdot I_{ij}^{sqr} + \sum_{s=1}^{S} P_{j,s}^c = \sum_{y=1}^{Y} m_{ij,y}^s \cdot \Delta P_{ij,y} + \sum_{y=1}^{Y} m_{ij,y}^s \cdot \Delta Q_{ij,y};\ \ \forall\, ij \in \Omega_l \tag{7}$$

In Equation (7), Y is the number of linearization blocks, $m_{ij,y}^s$ is the slope of the y_{th} block of the power flow at circuit ij; $\Delta P_{ij,y}$ and $\Delta Q_{ij,y}$ represent the values of the y_{th} block of P_{ij} and Q_{ij}, respectively.

Equations (8)–(12) are complementary expressions used in the linearization of the left-hand side of Equation (7). Equation (8) indicates the minimum and maximum limits of V_j^{sqr} taking into account the discretization steps. In this case, $x_{j,s}$ is a binary variable used in the discretization of V_j^{sqr}, ΔV is the discretization step, and S is the number of discretizations. Equation (9) represents the limit of the power discretization steps, where $P_{j,s}^c$ is the correction used in V^{sqr} times I_{sqr}. Equation (10) indicates the limits of $P_{j,s}^c$, and Equations (11) and (12) represent the limits of the binary variable $x_{j,s}$ and its nature, respectively.

$$\underline{V}^2 + \sum_{s=1}^{S} \left(\Delta V \cdot x_{j,s} \right) \leq V_j^{sqr} \leq \underline{V}^2 + \sum_{s=1}^{S} \left(\Delta V \cdot x_{j,s} \right) + \Delta V;\ \ \forall\, j \in \Omega_b \tag{8}$$

$$0 \leq \Delta V \cdot I_{ij}^{sqr} - P_{j,s}^c \leq \Delta V \cdot \sum_{c \in \Omega_c} \overline{I}_c^2 \cdot W_{ij,c} \cdot \left(1 - x_{j,s} \right);\ \ \forall\, ij \in \Omega_l, \forall\, s \in 1..S \tag{9}$$

$$0 \leq P_{j,s}^c \leq \Delta V \cdot \sum_{c \in \Omega_c} \overline{I}_c^2 \cdot W_{ij,c} \cdot x_{j,s};\ \forall\, ij \in \Omega_l \tag{10}$$

$$x_{j,s} \leq x_{j,s-1}; \ \ \forall\, j \in \Omega_b; \forall\, s \in 2..S \tag{11}$$

$$x_{j,s} \in \{0,1\}; \ \ \forall\, j \in \Omega_b; \forall\, s \in 1..S \tag{12}$$

Equations (13)–(19) serve the purpose of linearizing the right-hand side of Equation (7). In this instance, P_{ij}^{+} and P_{ij}^{-} are applied to determine $\left|P_{ij}\right|$, and Q_{ij}^{+} and Q_{ij}^{-} are employed to determine $\left|Q_{ij}\right|$, with $\overline{\Delta S}ij$ denoting the upper limit for each load flow block on branch ij. Equation (19) enforces the non-negativity of auxiliary variables Pij^{+}, P_{ij}^{-}, Q_{ij}^{+}, and Q_{ij}^{-}.

$$P_{ij}^{+} - P_{ij}^{-} = P_{ij}; \ \ \forall\, ij \in \Omega_l \tag{13}$$

$$Q_{ij}^{+} - Q_{ij}^{-} = Q_{ij}; \ \ \forall\, ij \in \Omega_l \tag{14}$$

$$P_{ij}^{+} + P_{ij}^{-} = \sum_{y=1}^{Y} \Delta P_{ij,y}; \ \ \forall\, ij \in \Omega_l \tag{15}$$

$$Q_{ij}^{+} + Q_{ij}^{-} = \sum_{y=1}^{Y} \Delta Q_{ij,y}; \ \ \forall\, ij \in \Omega_l \tag{16}$$

$$0 \leq \Delta P_{ij,y} \leq \overline{\triangle S}_{ij}; \ \ \forall\, ij \in \Omega_l, \forall\, y \in 1..Y \tag{17}$$

$$0 \leq \Delta Q_{ij,y} \leq \overline{\triangle S}_{ij}; \ \ \forall\, ij \in \Omega_l, \forall\, y \in 1..Y \tag{18}$$

$$P_{ij}^{+}, P_{ij}^{-}, Q_{ij}^{+}, Q_{ij}^{-} \geq 0; \ \ \forall\, ij \in \Omega_l \tag{19}$$

2.6. Constraints Associated with the ODNR

Equations (20) to (26) model the ODNR problem taking into account the OCS. The upper limits of auxiliary variables P_{ij}^{+} and P_{ij}^{-} are given by Equations (20) and (21), respectively. The reactive power flow limit in branch ij is given by Equation (22). Equation (23) indicates the limits of b_{ij}; which is zero if the circuit ij is closed; otherwise, the value of b_{ij} is defined by Equation (23). Equation (24) defines the condition of radiality of the PDS, and N is the number of buses of the PDS. Equation (25) indicates that if there is power flow in branch ij, it must have only one direction. Therefore, if $y_{ij}^{+} = 1$, it follows that $y_{ij}^{-} = 0$ and vice versa; otherwise, when $y_{ij}^{+} = 0$ and $y_{ij}^{-} = 0$, the circuit is open (there is no power flow). Equation (26) denotes the binary nature of y_{ij}^{+} and $+y_{ij}^{-}$.

$$P_{ij}^{+} \leq \overline{V} \cdot \ \overline{I}_{ij,c} \cdot W_{ij,c} \cdot y_{ij}^{+}; \ \ \forall ij \in \Omega_l; \ \forall ij \in \Omega_l \tag{20}$$

$$P_{ij}^{-} \leq \overline{V} \cdot \overline{I}_{ij,c} \cdot W_{ij,c} \cdot y_{ij}^{-}; \ \ \forall ij \in \Omega_l; \ \forall ij \in \Omega_l \tag{21}$$

$$|Q_{ij}| \leq \overline{V} \cdot \overline{I}_{ij,c} \cdot W_{ij,c} \cdot \left(y_{ij}^{+} + y_{ij}^{-}\right); \ \ \forall ij \in \Omega_l \tag{22}$$

$$|b_{ij}| \leq \left(\overline{V}^2 - \underline{V}^2\right)\left(1 - \left(y_{ij}^{+} + y_{ij}^{-}\right)\right); \ \ \forall ij \in \Omega_l \tag{23}$$

$$\sum_{\forall ij \in \Omega_l} \left(y_{ij}^{+} + y_{ij}^{-}\right) = N - 1; \ \ \forall ij \in \Omega_l \tag{24}$$

$$\left(y_{ij}^{+} + y_{ij}^{-}\right) \leq 1; \ \ \forall ij \in \Omega_l \tag{25}$$

$$y_{ij}^{+}, \ y_{ij}^{-} \in \{0,1\}; \ \ \forall ij \in \Omega_l \tag{26}$$

2.7. Constraints Associated with the OCS

Equations (27) and (28) are used in the OCS problem, and define, respectively, the possible values of the variable $W_{ij,c}$ and its binary nature.

$$\sum_{c \in \Omega_c} W_{ij,c} \leq \left(y_{ij}^{+} + y_{ij}^{-}\right); \ \ \forall ij \in \Omega_l \tag{27}$$

$$W_{ij,c} \ \text{ binary}; \ \ \forall ij \in \Omega_l, \ \forall c \in \Omega_c \tag{28}$$

The expressions given by Equations (29) and (30) are used to determine the input parameters of the objective function. In this case, the constant parameters presented in Equation (29) are taken from [8]. The system loss factor LF is calculated with the demand factor (DF), as indicated in Equation (29), whereas CRF is the capital recovery factor, which is calculated considering the interest rate (i) and the number of years (n) envisaged in the distribution planning, as indicated in Equation (30).

$$LF = 0.16 \cdot DF + 0.84 \cdot DF^2 \tag{29}$$

$$CRF = \frac{i(i+1)^n}{(i+1)^n - 1} \tag{30}$$

Constraints (31) and (32) define the upper and lower limits of each block's contribution to $|P_{ij}|$ and $|Q_{ij}|$, respectively, where ΔS_{ij} is the upper limit of each block of the power flow at circuit ij.

$$m^s_{ij,y} = (2y-1)\Delta S_{ij} \tag{31}$$

$$\Delta S_{ij} = \overline{V} \cdot \overline{I}_{ij}/Y \tag{32}$$

3. Integration of ODNR and OCS via Mixed Integer Linear Programming Model

Equations (1) to (28) represent a MINLP problem. The linearizations that allow recasting this model into a MILP problem are presented in this section. Equations (1) to (4) are nonlinear due to the multiplication of the variables $W_{ij,c} \cdot I^{sqr}_{ij}$. This product of a binary and continuous variable is labeled as $\phi_{ij,c}$. The process of linearizing this expression can be accomplished through the utilization of the big-M method (where M represents a suitably large value), exemplified in Equations (33) and (34).

$$0 \leq -\phi_{ij,c} + I^{sqr}_{ij} \leq M \cdot \left(1 - W_{ij,c}\right) \tag{33}$$

$$0 \leq \phi_{ij,c} \leq M \cdot W_{ij,c} \tag{34}$$

The voltage drop in the branches of the PDS defined by Equation (4) is nonlinear due to the multiplications of $W_{ij,c} \cdot P_{ij}$ and $W_{ij,c} \cdot Q_{ij}$. These nonlinearities can be converted into linear forms using the big-M approach, as illustrated in Equations (35) through (38). In this case, the products $W_{ij,c} \cdot P_{ij}$ and $W_{ij,c} \cdot Q_{ij}$ are labeled as new continuous variables $\beta_{ij,c}$ and $\delta_{ij,c}$, respectively.

$$0 \leq -\beta_{ij,c} + P_{ij} \leq M \cdot \left(1 - W_{ij,c}\right) \tag{35}$$

$$0 \leq \beta_{ij,c} \leq M \cdot W_{ij,c} \tag{36}$$

$$0 \leq -\delta_{ij,c} + Q^{sqr}_{ij} \leq M \cdot \left(1 - W_{ij,c}\right) \tag{37}$$

$$0 \leq \delta_{ij,c} \leq M \cdot W_{ij,c} \tag{38}$$

Equations (6) and (20) to (22) are nonlinear due to the multiplication of binary variables $W_{ij,c} \cdot y^+_{ij}$ and $W_{ij,c} \cdot y^-_{ij}$. These multiplications are renamed using new binary variables labeled as $U^+_{ij,c}$ and $U^-_{ij,c}$, respectively. The linearization of these expressions is indicated by Equations (39) to (44).

$$0 \leq U^+_{ij,c} \leq W_{ij,c} \tag{39}$$

$$0 \leq U^+_{ij,c} \leq y^+_{ij} \tag{40}$$

$$W_{ij,c} + y^+_{ij} - 1 \leq U^+_{ij,c} \leq 1 \tag{41}$$

$$0 \leq U^-_{ij,c} \leq W_{ij,c} \tag{42}$$

$$0 \leq U^{-}_{ij,c} \leq y^{-}_{ij} \tag{43}$$

$$W_{ij,c} + y^{-}_{ij} - 1 \leq U^{-}_{ij,c} \leq 1 \tag{44}$$

Equations (9) and (10) are nonlinear due to the multiplication of binary variables $W_{ij,c} \cdot x_{j,s}$. This multiplication is renamed using the binary variable $A_{ij,c,s}$, and its linearization is performed as shown in Equations (45) to (47).

$$0 \leq A_{ij,c,s} \leq W_{ij,c} \tag{45}$$

$$0 \leq A_{ij,c,s} \leq x_{j,s} \tag{46}$$

$$W_{ij,c} + x_{j,s} - 1 \leq A_{ij,c,s} \leq 1 \tag{47}$$

Following the linearizations presented above, the objective function (see Equation (1)) is reformulated as shown in Equation (48).

$$\text{Minimize } f = k_c \sum_{\forall ij \in \Omega_l} \sum_{\forall c \in \Omega_c} L_{ij} \cdot R_c \cdot \phi_{ij,c} + CRF \sum_{\forall ij \in \Omega_l} \sum_{\forall c \in \Omega_c} L_{ij} \cdot C_c \cdot W_{ij,c} \tag{48}$$

The power balance constraints (Equations (2) and (3)) are also modified as follows:

$$\sum_{\forall ki \in \Omega_l} P_{ki} - \sum_{\forall ij \in \Omega_l} P_{ij} - \sum_{\forall ij \in \Omega_l} \sum_{\forall c \in \Omega_c} \left(L_{ij} \cdot R_c \cdot \phi_{ij,c} \right) + P^s_i = P^d_i; \ \ \forall i \in \Omega_b \tag{49}$$

$$\sum_{\forall ki \in \Omega_l} Q_{ki} - \sum_{\forall ij \in \Omega_l} Q_{ij} - \sum_{\forall ij \in \Omega_l} \sum_{\forall c \in \Omega_c} \left(L_{ij} \cdot X_c \cdot \phi^{sqr}_{ij} \right) + Q^s_i = Q^d_i; \ \ \forall i \in \Omega_b \tag{50}$$

The voltage drops in branches (Equation (4)) are rewritten as follows:

$$V^{sqr}_i - V^{sqr}_j = 2 \cdot L_{ij} \sum_{\forall c \in \Omega_c} \left(R_c \cdot \beta_{ij,c} + X_c \cdot \delta_{ij,c} \right) + L^2_{ij} \cdot Z^2_c \cdot \phi_{ij,c} + b_{ij}; \ \ \forall ij \in \Omega_l \tag{51}$$

The current limit given by Equation (6) is rewritten as indicated in Equation (52)

$$0 \leq I^{sqr}_{ij} \leq \sum_{c \in \Omega_c} \overline{I}^2_{ij,c} \left(U^{+}_{ij,c} + U^{-}_{ij,c} \right); \ \ \forall \, ij \in \Omega_l \tag{52}$$

Equations (9) and (10) are rewritten as indicated in Equations (53) and (54).

$$0 \leq \Delta V \cdot I^{sqr}_{ij} - P^c_{j,s} \leq \Delta V \cdot \sum_{c \in \Omega_c} \left(\overline{I}^2_c \cdot W_{ij,c} - A_{ij,c} \right); \ \ \forall \, ij \in \Omega_l, \forall \, s \in 1..S \tag{53}$$

$$0 \leq P^c_{j,s} \leq \Delta V \cdot \sum_{c \in \Omega_c} \overline{I}^2_c \cdot A_{ij,c}; \ \forall \, ij \in \Omega_l \tag{54}$$

Equations (55) to (57) indicate the linearization of Equations (6), and (20) to (22), respectively.

$$P^{+}_{ij} \leq \overline{V} \cdot \ \overline{I}_{ij,c} \cdot U^{+}_{ij,c}; \ \ \forall ij \in \Omega_l; \ \forall ij \in \Omega_l \tag{55}$$

$$P^{-}_{ij} \leq \overline{V} \cdot \overline{I}_{ij,c} \cdot U^{-}_{ij,c}; \ \ \forall ij \in \Omega_l; \ \forall ij \in \Omega_l \tag{56}$$

$$|Q_{ij}| \leq \overline{V} \cdot \overline{I}_{ij,c} \cdot \left(U^{+}_{ij,c} + U^{-}_{ij,c} \right); \ \ \forall ij \in \Omega_l \tag{57}$$

Finally, using the proposed linearization approach, the initial MINLP model given by Equations (1) to (28) can be represented as a MILP model as indicated below:

$$\text{Minimize } \ (48) \tag{58}$$

$$\text{Subject to: } \ (49), (50), (51), (5), (7), (8), (11)–(19), \ (23)–(28), (33)–(47), (52)–(57) \tag{59}$$

4. Test and Results

The simultaneous implementation of ODNR and OCS was simulated using AMPL 4.23 and solved using the standard settings in CPLEX 22.1.1.0. The effectiveness of the proposed model is illustrated using 32-, 69-, and 83-bus test systems. Each of these test systems is evaluated under six distinct scenarios:

- Initial scenario (base case).
- Optimal conductor selection (only OCS).
- Optimal distribution network reconfiguration (only ODNR).
- ODNR and then OCS (sequential approach).
- OCS and then ODNR (sequential approach).
- Simultaneous OCS and ODNR.

Table 1 presents the conductor types used for all test systems, taken from [22], and Table 2 indicates the parameters adopted for the objective function, which are based on [8].

Table 1. Available conductor types for all test systems.

Conductor Type	Name	Area mm^2	R [Ω/km]	X [Ω/km]	Imax [A]	Cost [US$/km]
1	Mole	6.5	2.7180	0.374	70	90
2	Squirrel	13	1.3740	0.355	120	170
3	Gopher	16	1.0980	0.349	130	210
4	Weasel	20	0.9116	0.345	150	260
5	Ferret	25	0.6795	0.339	175	340
6	Rabbit	30	0.5449	0.335	200	420
7	Mink	40	0.4565	0.353	250	500
8	Horse	42	0.3977	0.327	270	540
9	Beaver	45	0.3841	0.327	257	590
10	Raccoon	48	0.3656	0.329	260	630
11	Otter	50	0.3434	0.328	270	770
12	Cat	55	0.3020	0.327	290	760
13	Dog	65	0.2745	0.315	305	820
14	Leopard	80	0.2193	0.282	395	1010
15	Coyote	80	0.2214	0.268	380	1040
16	Tiger	80	0.2221	0.271	385	1130
17	Wolf	95	0.1844	0.266	425	1370
18	Lynx	110	0.1589	0.261	470	1590
19	Panther	130	0.1375	0.256	510	1840
20	Lion	140	0.1223	0.252	560	2060

Table 2. Objective function parameters for all simulations.

Parameter	Value
k_p [U$/kW]	1.04
K_e [U$/kWh]	0.012
T (hours)	8760
DF	0.4019
i (%)	8
n (year)	20

There are several benchmark test systems used to evaluate the effectiveness of the ODNR problem. However, due to the nature of ODNR, these systems only provide data on the resistance and reactance of conductors. Crucial information such as the length of feeder sections and conductor costs is not specified, which is necessary to solve the OCS problem. To combine the ODNR and OCS problems, we use the information in Table 1, reported in [22]; although other conductor-type tables that exist in the specialized literature may also be used. The original conductors of the test systems were substituted with their counterparts from Table 1, while adjusting the distances between nodes to ensure similar results compared to those of the original systems. Following the conductor replacement, a power flow analysis was carried out to assess the active power losses and minimum voltage in the test systems.

Table 3 compares the original values of active power losses and minimum voltage magnitudes for each test system with respect to those obtained after updating the conductor types from Table 1. In both cases, the minimum voltage magnitudes were obtained at the same buses for the original test systems. The new conductor types used in the test systems are indicated in Appendix A. Notably, the errors with the new conductor data range from 0.03% to 3.58%, confirming the equivalence between the original and proposed system data.

Table 3. Base case results of the test systems considering conductors of Table 1.

Test System	Active Power Losses [kW]			Minimum Voltage [p.u.]		
	Original	Proposed	Error [%]	Original	Proposed	Error [%]
33-bus	202.67	203.23	0.27	0.9131	0.9128	0.03
69-bus	224.99	233.04	3.58	0.9092	0.8919	1.90
83-bus	531.99	515.77	3.04	0.9285	0.9514	2.46

4.1. OCS and ODNR for the 33-Bus Test System

The 33-bus test system comprises 37 branches, 32 normally closed tie switches, and 5 initially open interconnection switches. The system operates at a nominal voltage of 12.66 kV and has a total demand of 3715 + j 2300 kVA. A power flow was computed to determine the initial state of the network. In the initial base case, the active power losses amount to 203.23 kW, and the minimum voltage magnitude is 0.9128 p.u. at bus 18. For reference, the voltage limits range from a minimum of 0.92 p.u. to a maximum of 1.00 p.u.

Table 4 displays the information of the base case as well as the solutions obtained for only OCS, only ODNR, sequential ODNR and then OCS, sequential OCS and then ODNR and simultaneous OCS and ODNR.

Table 4. Proposed solutions for the 33-bus test system.

Description	Base Case	Only ODNR	Only OCS	Sequential ODNR → OCS	Sequential OCS → ODNR	Simultaneous OCS and ODNR
Minimum voltage [p.u]	0.9128	0.9294	0.9500	0.9600	0.9658	0.9689
Active power losses [kW]	203.23	161.72	79.44	65.37	70.79	63.85
Active power losses cost [$]	4483.72	3567.91	1752.68	1442.23	1561.79	1408.68
Conductor cost [$/year]	661.49	692.98	1441.16	1431.81	1435.65	1277.24
Total cost [$/year]	5145.21	4260.89	3193.84	2874.01	2997.44	2685.92
Economic benefit [%]	0.00	17.18	37.92	44.14	41.74	47.80

Based on the findings presented in Table 4, it is evident that the simultaneous implementation of OCS and ODNR provides the highest economic benefit of 47.8%. Individually, the ODNR yields an economic benefit of 17.18%, whereas the OCS achieves a benefit of 37.92%. Furthermore, when sequential strategies of the ODNR and then OCS or vice versa are implemented, the economic benefits are 44.14% and 41.74%, respectively. Note that the improvement of these strategies is superior with respect to any single strategy; nonetheless, they are lower than the one obtained with the simultaneous strategy.

In terms of technical losses, the simultaneous implementation of OCS and ODNR, once again, yields the highest reduction rate at 68.58%. Individually, ODNR and OCS result in loss reductions of 20.43% and 60.9%, respectively. Regarding the voltage profile, the initial scenario, referred to as the base case, presents a minimum voltage of 0.9128 p.u. The most substantial enhancement in the voltage profile was attained by implementing the simultaneous OCS and ODNR, contrasting with the base case. In this situation, there was a 5.47% increase in the minimum voltage.

It was then demonstrated that the simultaneous combination of the two optimization approaches, OCS and ODNR, leads to a more optimized system (with minimal losses and investment costs) than when any of them is solved either individually or sequentially.

Table 5 indicates the open switches used in the analyzed cases. It is important to highlight that the open switches in the ODNR-only scenario are distinct from those employed in the simultaneous OCS and ODNR case; nonetheless, they coincide with the sequential scenario of ODNR and then OCS. The reason for this disparity lies in the impact of the OCS on the most efficient reconfiguration strategy aimed at minimizing losses.

Table 5. Open switches for the 33-bus test system.

Case	Open Switches
Base case	33 to 37
Only OCS	33 to 37
Only ODNR	9, 14, 32, 33, 37
Sequential ODNR-OCS	9, 14, 32, 33, 37
Sequential OCS-ODNR	9, 14, 28, 32, 33
Simultaneous OCS and ODNR	14, 28, 33, 35, 36

Table 6 presents the conductor types selected for the base case (A), only OCS (B), sequential ODNR and then OCS (C) and simultaneous OCS and ODNR (D). Note that the solutions differ significantly due to the impact of the ODNR. As the system reconfiguration is optimized, there are changes in the OCS, and this leads to a decrease in the investment conductor cost (see Table 4).

Table 6. Selected conductors for all simulations carried out for the 33-bus test system.

Branch	A	B	C	D	Branch	A	B	C	D	Branch	A	B	C	D
1	15	20	20	20	14	2	2	–	–	27	2	8	8	1
2	15	20	20	20	15	2	2	4	2	28	2	8	8	–
3	7	18	18	14	16	2	2	3	1	29	2	8	8	8
4	7	18	14	13	17	2	1	3	1	30	2	4	5	4
5	7	14	14	13	18	1	3	8	3	31	2	2	3	2
6	2	8	8	8	19	1	2	6	2	32	2	1	–	1
7	2	8	8	8	20	1	1	5	1	33	2	2	–	–
8	2	8	5	6	21	1	1	4	1	34	2	2	5	2
9	2	6	–	3	22	2	8	8	14	35	2	2	3	–
10	2	5	1	3	23	2	8	8	14	36	2	2	1	–
11	2	5	1	2	24	2	4	4	14	37	2	2	–	8
12	2	5	2	2	25	2	13	13	1					
13	2	3	1	1	26	2	13	8	1					

A: base case; B: only OCS; C: sequential ODNR-OCS, and D: simultaneous OCS and ODNR.

Figure 1 depicts the optimal solution for the simultaneous OCS and ODNR problem, where the conductor type of each branch is indicated in parenthesis in red, and the branch number is indicated in blue. Note that the solution involved the use of conductor types 20, 14, 13, 8, 6, 4, 3, 2, and 1. Larger capacity conductors were selected for branches located closer to the substation. Furthermore, Figure 1 also shows the specific switches that were opened to achieve the optimal reconfiguration of the system.

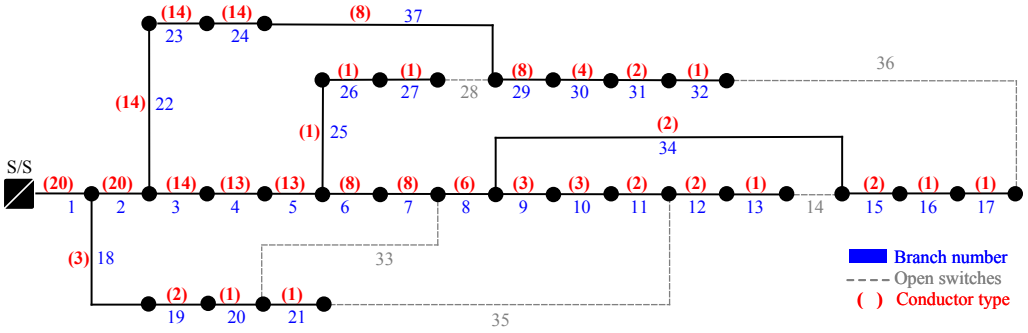

Figure 1. Simultaneous OCS and ODNR for the 33-bus test system.

Figure 2 illustrates the voltage profile of the 33-bus test system for the different cases under study. Note that the simultaneous OCS and ODNR improves the voltage profile, especially at buses far away from the substation.

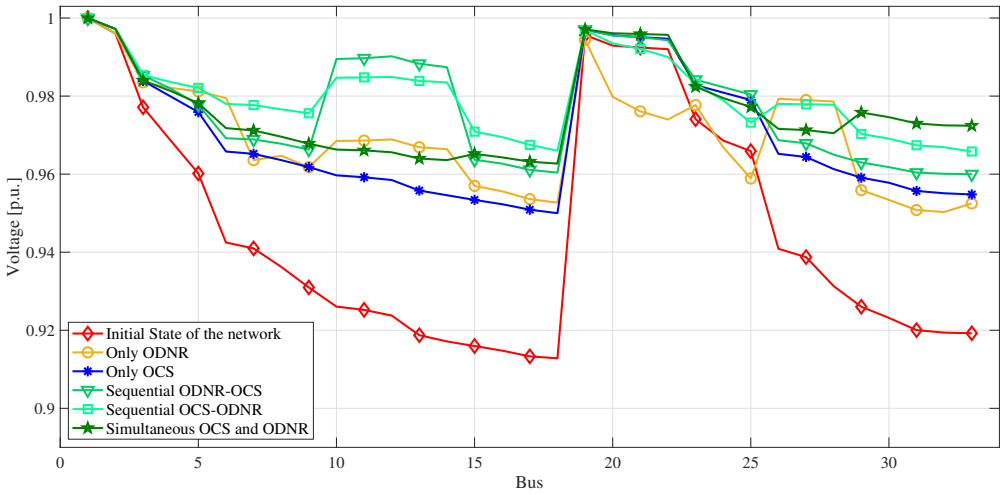

Figure 2. Voltage profile of the 33-bus test system for all simulations carried out.

According to Figure 2, buses 13 to 18 and 30 to 33 exhibit low voltage values in the base case. However, this issue is effectively rectified through the implementation of simultaneous OCS and ODNR (indicated by the green line). With this solution, all voltage magnitudes are maintained above 0.96 p.u. Furthermore, the overall voltage profile is significantly improved with the simultaneous implementation of OCS and ODNR.

4.2. OCS and ODNR for the 69-Bus Test System

The 69-bus test system has 73 branches, 68 normally closed tie switches, and 5 initially open interconnection switches. The system operates at a nominal voltage of 12.66 kV with a total demand of 3802 + j 2694 kVA. A power flow was calculated to find the initial state of the network. In the initial state, active power losses are 230.78 kW, and the minimum voltage magnitude of the system is 0.8973 p.u. at bus 65. Voltage limits are considered between 0.95 and 1.00 p.u. Table 7 presents the results obtained with the 69-bus test system.

Table 7. Proposed solutions for the 69-bus test system.

Description	Base Case	Only ODNR	Only OCS	Sequential ODNR → OCS	Sequential OCS → ODNR	Simultaneous OCS and ODNR
Minimum voltage [p.u]	0.8919	0.9123	0.9500	0.9500	0.9546	0.9725
Active power losses [kW]	233.04	174.61	71.00	69.84	64.22	34.4
Active power losses cost [$]	5141.40	3852.30	1566.47	1540.97	1372.72	759.97
Conductor cost [$/year]	880.11	873.90	2594.36	1878.94	2574.92	687.67
Total cost [$/year]	6021.51	4726.20	4160.83	3419.91	3947.64	1447.64
Economic benefit [%]	0.00	21.51	30.90	43.21	34.44	75.96

The results reported in Table 7 show that the simultaneous implementation of OCS and ODNR provides the highest economic benefit of 75.96%. Individually, OCS yields an economic benefit of 30.9%, whereas ODNR achieves 21.51%. Furthermore, the sequential optimization of ODNR and then OCS and vice versa yield economic benefits of 43.21% and 34.44% respectively.

The simultaneous implementation of OCS and ODNR also presents the highest reduction in power loss. Note that the power losses of the base case amount to 233.04 kW, whereas the ones obtained with the simultaneous optimization are 34.4 kW, representing a reduction of 85.23%. Individually, ODNR and OCS result in loss reductions of 66.0% and 58.3%, respectively, whereas the sequential optimization resulted in power loss reductions

of 70.03% and 72.44% for ODNR and then OCS, and vice versa, respectively. Regarding the voltage profile, the initial scenario, referred to as the base case, presents a minimum voltage of 0.8919 p.u. The most substantial enhancement in voltage profile was attained by simultaneously implementing OCS and ODNR, with a minimum voltage of 0.9725 p.u. In this situation, there was an 8.26% increase in the minimum voltage. Finally, the results for this test system show that the combination of the two optimization approaches, OCS and ODNR, leads to a more optimized system than when any of them are solved individually.

Table 8 indicates the open switches used in the analyzed cases. Note that the open switches in the ODNR-only scenario are the same as the ones of the sequential ODNR-OCS scenario, but different from those employed in the simultaneous OCS and ODNR scenario. This is due to the impact of the OCS on the most efficient reconfiguration strategy aimed at minimizing losses.

Table 8. Open switches for the 69-bus test system.

Case	Open Switches
Initial base case	69 to 73
Only OCS	69 to 73
Only ODNR	13, 20, 61, 69, 72
Sequential ODNR-OCS	13, 20, 61, 69, 72
Sequential OCS-ODNR	12, 64, 69, 70, 72
Simultaneous OCS and ODNR	20, 56, 69, 71, 73

Table 9 presents the conductor types selected for the base case (A), only OCS (B), sequential ODNR and then OCS (C) and simultaneous OCS and ODNR (D). The solutions differ significantly due to the impact of the ODNR. As the system reconfiguration is optimized, there are changes in the OCS, leading to a decrease in the investment conductor cost. Consequently, integrating OCS and ODNR in an optimization problem results in a more efficient and economically viable distribution system planning.

Figure 3 depicts the optimal solution for the simultaneous OCS and ODNR problem, where the conductor type of each branch is indicated in parenthesis in red, and the branch number is indicated in blue. Note that the solution involves the use of conductor types 20, 14, 8, 6, 3, 2, and 1. It was observed that larger capacity conductors are selected for branches located closer to the substation. Furthermore, Figure 3 also shows the specific switches that were opened to achieve the optimal reconfiguration of the system.

Figure 4 illustrates the voltage profile of the 69-bus test system considering the cases described in Table 7. Note that in the base case buses 60 to 66 exhibit low voltage values. However, this issue is effectively rectified through the implementation of OCS and ODNR. An initial improvement in these voltages is obtained with only ODNR, as indicated in the yellow line, these voltages are further improved with only OCS and with the sequential implementation of both. Finally, it is observed that the best voltage profile is obtained with the simultaneous OCS and ODNR. In this case, all voltage magnitudes remain above 0.97 p.u.

Table 9. Selected conductors for all simulations carried out for the 69-bus test system.

Branch	A	B	C	D	Branch	A	B	C	D	Branch	A	B	C	D
1	14	20	20	20	26	1	1	3	1	51	1	1	1	1
2	14	20	19	20	27	1	1	1	1	52	6	20	14	1
3	14	20	20	20	28	1	1	1	1	53	6	19	14	1
4	14	20	20	8	29	1	1	1	1	54	6	20	14	1
5	14	20	20	8	30	1	1	1	1	55	6	19	14	1
6	14	20	20	8	31	1	1	1	1	56	6	19	14	–
7	14	20	19	8	32	1	1	1	1	57	6	19	14	1
8	14	20	19	8	33	1	1	1	1	58	6	19	14	1
9	2	8	8	8	34	1	1	1	1	59	5	19	14	14
10	2	8	8	8	35	1	2	3	2	60	5	19	14	14
11	2	6	8	6	36	1	1	3	1	61	1	8	–	3
12	2	3	5	3	37	1	1	3	1	62	1	10	1	3
13	2	3	–	1	38	1	1	3	1	63	1	8	1	3
14	2	3	1	1	39	1	1	3	1	64	1	4	2	1
15	2	3	1	1	40	1	1	2	1	65	1	1	1	1
16	2	3	1	1	41	1	1	2	1	66	1	1	1	1
17	2	2	1	1	42	1	1	2	1	67	1	1	1	1
18	2	2	1	1	43	1	1	2	1	68	1	1	1	1
19	2	2	1	1	44	1	1	2	1	69	1	1	–	–
20	1	2	4	–	45	1	1	2	1	70	1	1	5	2
21	1	1	–	1	46	2	8	8	14	71	1	1	1	–
22	1	1	4	1	47	2	8	8	14	72	1	1	–	14
23	1	1	4	1	48	2	8	8	14	73	1	1	3	–
24	1	1	3	1	49	2	4	4	14					
25	1	1	3	1	50	1	1	1	1					

A: Base case; **B**: only OCS; **C**: sequential ODNR-OCS, and **D**: simultaneous OCS and ODNR.

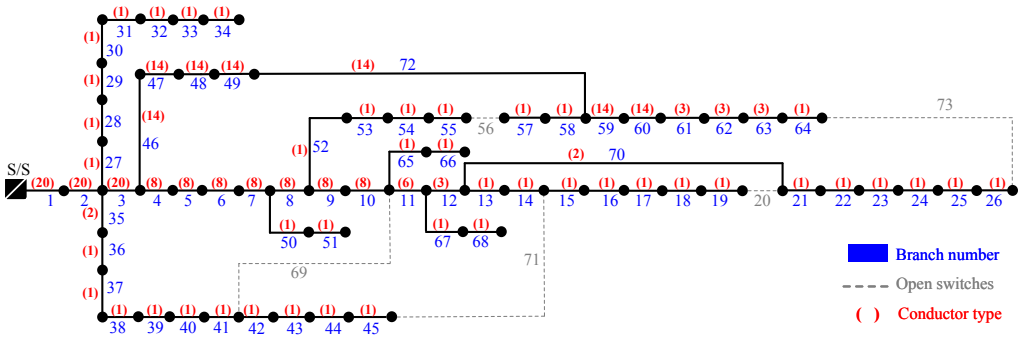

Figure 3. Simultaneous OCS and ODNR for the 69-bus test system.

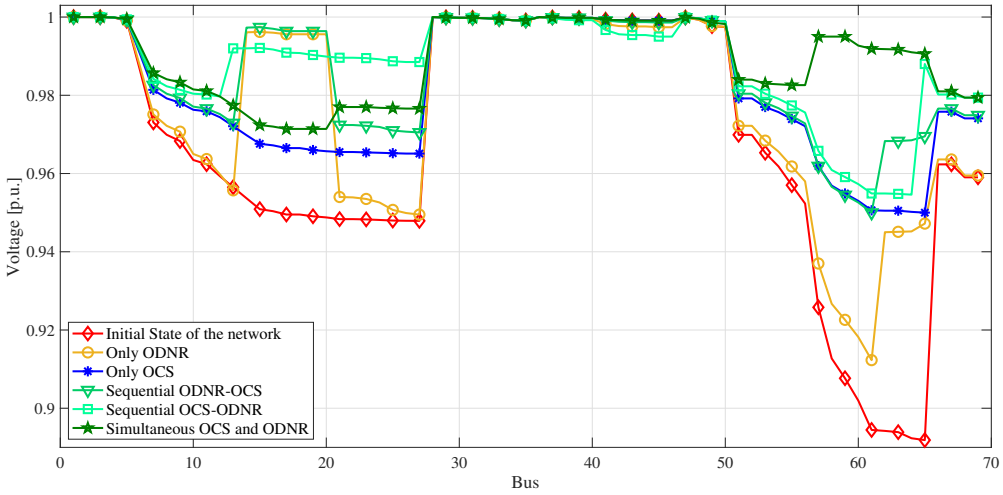

Figure 4. Voltage profile of the 69-bus test system for different scenarios.

4.3. OCS and ODNR for the 83-Bus Test System

The 83-bus test system comprises 96 branches, 83 normally closed tie switches, and 13 initially open interconnection switches. The system operates at a nominal voltage of 11.4 kV and has a total demand of 28,350.9 + j 20,700 kVA. A power flow was computed to determine the initial state of the network. In the initial base case, the active power losses are 531.91 kW, and the minimum voltage magnitude is 0.9378 p.u. In this case, voltage limits are considered from 0.95 to 1.00 p.u. Table 10 presents the optimal solutions found with the 83-bus test system for the different cases under study.

Table 10. Proposed solutions for the 83-bus test system.

Description	Base Case	Only ODNR	Only OCS	Sequential ODNR → OCS	Sequential OCS → ODNR	Simultaneous OCS and ODNR
Minimum voltage [p.u.]	0.9514	0.9733	0.9605	0.9799	0.9817	0.9605
Active power losses [kW]	515.77	491.33	263.72	251.79	255.45	253.23
Active power losses cost [$]	11,379.07	10,839.87	5818.36	5555.06	5635.81	5586.81
Conductor cost [$/year]	2134.76	2245.92	4136.38	4338.42	4164.07	4100.23
Total cost [$/year]	13,513.83	13,085.79	9954.75	9893.58	9799.88	9687.04
Economic benefit [%]	0.00	3.17	26.34	26.78	27.48	28.31

From Table 10, it is evident that the simultaneous implementation of OCS and ODNR provides the highest economic benefit of 28.31%. This benefit is closely followed by the one obtained with sequential OCS and then ODNR of 27.48%. It was also observed that the sequential ODNR and then OCS present similar economic benefits of only OCS with 26.78% and 26.34%, respectively. This means that for this test system, it is difficult to further reduce power losses once OCS has been carried out. Finally, the lowest economic benefit of only 3.17% was achieved with only ODNR.

As regards technical losses, the ODNR offers a reduction of only 4.73% (from 515.77 kW of the base case to 491.33 kW), whereas the rest of the cases under study manage to reduce power losses by nearly 50%. In this case, the highest power loss reduction was obtained with the sequential ODNR and then OCS approach (51.18%) followed by the simultaneous approach (50.9%). It is worth mentioning that despite the fact that this sequential approach presented a higher power loss reduction, the overall economic benefit of the simultaneous approach is higher.

Regarding the voltage profile, the initial scenario, referred to as the base case, presents a minimum voltage of 0.9514 p.u. The most substantial enhancement in the voltage profile was attained by the sequential OCS and then ODNR approach. In this situation, the minimum voltage is 0.9817 p.u.; on the other hand, the minimum voltage attained by the simultaneous approach was 0.9605 p.u.

Table 11 indicates the open switches used in the analyzed cases. It is important to highlight that the open switches in the ODNR-only scenario are distinct from those employed in the simultaneous OCS and ODNR scenarios but the same as the sequential ODNR and then OCS scenario. This is due to the impact of the OCS on the most efficient reconfiguration strategy aimed at minimizing power losses.

Table 11. Open switches for 83-bus test system.

Case	Open Switches
Initial base case	84 to 96
Only OCS	84 to 96
Only ODNR	7, 13, 34, 39, 42, 63, 72, 83, 84, 86, 89, 90, 92
Sequential ODNR-OCS	7, 13, 34, 39, 42, 63, 72, 83, 84, 86, 89, 90, 92
Sequential OCS-ODNR	7, 32, 34, 35, 41, 64, 72, 83, 84, 86, 88, 89, 90
Simultaneous OCS and ODNR	32, 39, 42, 72, 83 84, 85, 86, 88, 89, 90, 94, 96

Table 12 presents the conductor types selected for the base case (A), only OCS (B), sequential ODNR and then OCS (C) and simultaneous OCS and ODNR (D). Note that the solutions differ significantly due to the impact of the ODNR. As the system reconfiguration is optimized, there are changes in the OCS, and this leads to a decrease in the investment conductor cost.

Table 12. Selected conductors for all simulations carried out for the 83-bus test system.

Branch	A	B	C	D	Branch	A	B	C	D	Branch	A	B	C	D
1	14	20	19	20	33	6	14	8	14	65	15	20	19	20
2	14	20	19	20	34	6	14	8	14	66	15	20	20	20
3	14	20	19	20	35	6	6	8	5	67	15	20	20	20
4	14	20	18	20	36	6	5	5	4	68	15	20	20	20
5	14	20	14	20	37	6	3	8	3	69	9	19	14	18
6	12	20	14	20	38	6	3	20	2	70	9	19	20	18
7	5	14	8	14	39	6	1	20	–	71	9	19	20	18
8	1	3	8	3	40	6	1	20	1	72	9	2	20	–
9	1	3	8	3	41	6	3	14	2	73	5	14	14	14
10	1	4	19	4	42	6	1	20	–	74	5	14	14	14
11	13	20	19	20	43	2	13	20	13	75	5	14	5	14
12	13	20	14	20	44	2	13	20	13	76	5	3	14	3
13	5	8	20	8	45	2	13	20	13	77	17	20	8	20
14	13	8	20	8	46	2	2	20	2	78	17	20	14	20
15	17	20	20	20	47	13	20	20	20	79	17	20	13	20
16	17	20	20	20	48	13	20	18	20	80	7	14	5	8

Table 12. *Cont.*

Branch	A	B	C	D	Branch	A	B	C	D	Branch	A	B	C	D
17	16	20	20	20	49	13	20	14	20	81	7	13	14	8
18	16	20	14	20	50	13	20	8	20	82	7	6	4	1
19	7	19	14	20	51	13	20	19	20	83	7	5	14	–
20	7	8	4	14	52	13	14	19	14	84	13	13	13	–
21	1	6	5	6	53	13	13	19	13	85	5	5	5	–
22	1	1	3	1	54	13	8	18	8	86	13	13	13	–
23	1	1	20	1	55	13	2	18	2	87	13	13	13	2
24	1	1	20	1	56	5	14	8	14	88	5	5	5	–
25	7	19	19	20	57	5	14	8	14	89	16	16	16	–
26	7	19	19	20	58	5	14	8	14	90	20	20	20	–
27	7	18	8	20	59	5	8	20	9	91	7	7	7	5
28	7	18	20	20	60	5	8	20	9	92	17	17	17	14
29	6	2	20	3	61	5	8	20	8	93	6	6	6	1
30	17	20	13	18	62	5	8	20	8	94	6	6	6	–
31	17	20	8	18	63	5	8	19	8	95	6	6	6	1
32	17	14	13	–	64	5	3	19	3	96	5	5	5	–

A: base case; **B**: only OCS; **C**: sequential ODNR-OCS, and **D**: simultaneous OCS and ODNR.

Figure 5 depicts the optimal solution for the simultaneous OCS and ODNR problem, where the conductor type of each branch is indicated in parenthesis in red, and the branch number is indicated in blue. Note that the solution involved the use of conductor types 20, 19, 14, 13, 11, 8, 6, 5, 4, 3, 2, and 1. Furthermore, as with the other test systems, larger capacity conductors were selected for branches near the substation. Figure 5 also shows the specific switches that were opened to achieve the optimal reconfiguration.

Figure 6 depicts the voltage profile of the 83-bus test system. Note that for the base case, all voltage magnitudes are above 0.95 p.u.; nonetheless, the voltage profile is further improved in all cases under study.

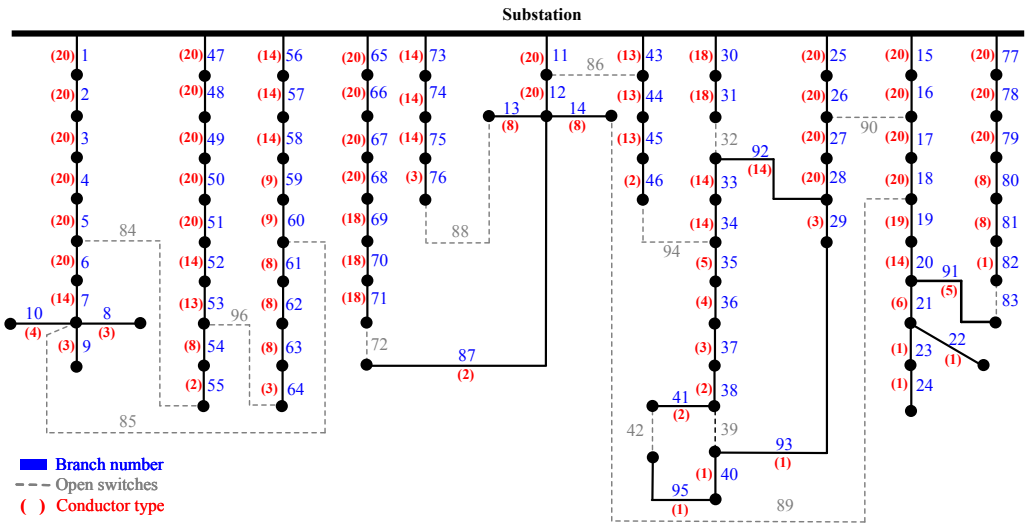

Figure 5. Simultaneous OCS and ODNR for the 83-bus test system.

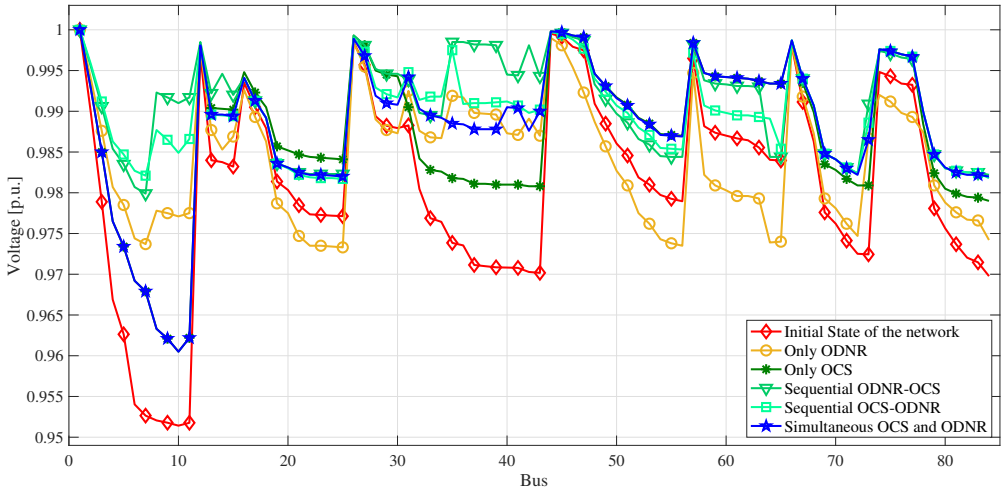

Figure 6. Voltage profile of the 83-bus test system

5. Conclusions

Choosing new conductors as replacements for outdated or deteriorated cables can lead to substantial reductions in power losses and enhancement of voltage profiles. Nevertheless, OCS alone might not always be fully effective in achieving significant reductions in technical losses or improving voltage profiles. As a result, OCS can be complemented using other technical approaches. In this study, we integrate OCS with ODNR, which is a method that modifies the distribution network's topology to minimize power losses and enhance voltage profiles.

Both OCS and ODNR were integrated into a unified MILP model, enabling to obtain globally optimal solutions. This marks the main innovation of the study because the integration of these two issues through a MILP approach has not been previously put forth in the specialized literature. Moreover, the model offers flexibility in decision making, allowing the problems to be addressed jointly or separately as needed.

The efficiency and suitability of the suggested model was assessed using three standard distribution test systems. In each investigated scenario, it was proven that employing simultaneously both optimization methods (OCS and ODNR) within the proposed MILP model results in a more optimized system, characterized by higher economic benefits, compared to solving either of them separately or sequentially.

In the 33-bus and 69-bus test systems, the combined application of OCS and ODNR yielded the greatest decrease in technical losses and the most notable enhancement in voltage profile. In the 83-bus test system the sequential ODNR and then OCS approach resulted in slightly higher power loss reduction than the simultaneous approach; nonetheless, the latter reported higher overall economic benefits. Additionally, across all test systems, implementing OCS and DNR simultaneously led to the choice of lower current capacity conductors compared to using only OCS. This capacity reduction was attributed to the effect of DNR and significantly influenced the overall investment cost. Future work may include a multi-period optimization approach to consider active and reactive power demand variations and the impact of renewable generation.

Author Contributions: Conceptualization, L.A.G.P., J.M.L.-L. and O.G.C.; data curation, L.A.G.P., J.M.L.-L. and O.G.C.; formal analysis, L.A.G.P., J.M.L.-L. and O.G.C.; funding acquisition, L.A.G.P., J.M.L.-L. and O.G.C.; investigation, L.A.G.P., J.M.L.-L. and O.G.C.; methodology, L.A.G.P., J.M.L.-L. and O.G.C.; project administration, L.A.G.P., J.M.L.-L. and O.G.C.; resources, L.A.G.P., J.M.L.-L. and O.G.C.; software, L.A.G.P., J.M.L.-L. and O.G.C.; supervision, L.A.G.P., J.M.L.-L. and O.G.C.; validation, L.A.G.P., J.M.L.-L. and O.G.C.; visualization, L.A.G.P., J.M.L.-L. and O.G.C.; writing—original draft, L.A.G.P., J.M.L.-L. and O.G.C.; writing—review and editing, L.A.G.P., J.M.L.-L. and O.G.C. All authors have read and agreed to the published version of the manuscript.

Funding: This work was funded by the Colombia Scientific Program within the framework of the called Ecosistema Científico (Contract No. FP44842- 218-2018), Universidad Tecnológica de Pereira (Risaralda, Colombia) and Universidad Estadual de Londrina (Paraná, Brasil).

Institutional Review Board Statement: Not applicable.

Informed Consent Statement: Not applicable.

Data Availability Statement: The data of this paper is available through e-mail via authors.

Acknowledgments: The authors would like to thank Universidad de Antioquia (Medellín, Colombia), Universidad Tecnologica de Pereira (Risaralda, Colombia) and Universidad Estadual de Londrina (Paraná, Brazil) for their support in the development of this work.

Conflicts of Interest: The authors declare no conflicts of interest.

Appendix A

The electrical data for the test systems used in this paper is provided in this section.

Table A1. Initial electrical data for the 33-bus test system.

Branch	Branch		P	Q	Conductor	Operation	Length	Branch	Branch		P	Q	Conductor	Operation	Length
	From	To	[kW]	[kVAr]	Type	State	[km]		From	To	[kW]	[kVAr]	Type	State	[km]
1	1	2	100	60	15	1	0.4164	20	20	21	90	40	1	1	0.1507
2	2	3	90	40	15	1	2.2267	21	21	22	90	40	1	1	0.2608
3	3	4	120	80	7	1	0.8018	22	3	23	90	50	2	1	0.3284
4	4	5	60	30	7	1	0.8348	23	23	24	420	200	2	1	0.6536
5	5	6	60	20	7	1	1.7941	24	24	25	420	200	2	1	0.6521
6	6	7	200	100	2	1	0.1362	25	6	26	60	25	2	1	0.1477
7	7	8	200	100	2	1	0.5178	26	26	27	60	25	2	1	0.2068
8	8	9	60	20	2	1	0.7496	27	27	28	60	20	2	1	0.7707
9	9	10	60	20	2	1	0.7598	28	28	29	120	70	2	1	0.5853
10	10	11	45	30	2	1	0.1431	29	29	30	200	600	2	1	0.3694
11	11	12	60	35	2	1	0.2725	30	30	31	150	70	2	1	0.7092
12	12	13	60	35	2	1	1.0684	31	31	32	210	100	2	1	0.2260
13	13	14	120	80	2	1	0.3942	32	32	33	60	40	2	1	0.2482
14	14	15	60	10	2	1	0.4301	32	32	33	60	40	2	1	0.2482
15	15	16	60	20	2	1	0.5432	33	8	21			2	0	1.4556
16	16	17	60	20	2	1	0.9381	34	9	15			2	0	1.4556
17	17	18	90	40	2	1	0.5328	35	12	22			2	0	1.4556
18	2	19	90	40	1	1	0.0603	36	18	33			2	0	0.3639
19	19	20	90	40	1	1	0.5534	37	25	29			2	0	0.3639

Table A2. Initial electrical data for the 69-bus test system.

Branch	Branch		P	Q	Conductor	Operation	Length	Branch	Branch		P	Q	Conductor	Operation	Length
	From	To	[kW]	[kVAr]	Type	State	[km]		From	To	[kW]	[kVAr]	Type	State	[km]
1	1	2	0.00	0.00	14	1	0.002	38	38	39	24.00	17.00	1	1	0.011
2	2	3	0.00	0.00	14	1	0.002	39	39	40	24.00	17.00	1	1	0.001
3	3	4	0.00	0.00	14	1	0.007	40	40	41	1.20	1.00	1	1	0.268
4	4	5	0.00	0.00	14	1	0.114	41	41	42	0.00	0.00	1	1	0.114
5	5	6	2.60	2.20	14	1	1.669	42	42	43	6.00	4.30	1	1	0.015
6	6	7	40.40	30.00	14	1	1.738	43	43	44	0.00	0.00	1	1	0.003
7	7	8	75.00	54.00	14	1	0.420	44	44	45	39.22	26.30	1	1	0.040
8	8	9	30.00	22.00	14	1	0.225	45	45	46	39.22	26.30	1	1	0.003
9	9	10	28.00	19.00	2	1	0.596	46	4	47	0.00	0.00	2	1	0.002
10	10	11	145.00	104.00	2	1	0.136	47	47	48	79.00	56.40	2	1	0.062
11	11	12	145.00	104.00	2	1	0.518	48	48	49	384.70	274.50	2	1	0.211

Table A2. *Cont.*

Branch	Branch		P	Q	Conductor	Operation	Length	Branch	Branch		P	Q	Conductor	Operation	Length
	From	To	[kW]	[kVAr]	Type	State	[km]		From	To	[kW]	[kVAr]	Type	State	[km]
12	12	13	8.00	5.50	2	1	0.750	49	49	50	384.70	274.50	2	1	0.060
13	13	14	8.00	5.50	2	1	0.760	50	8	51	40.50	28.30	1	1	0.034
14	14	15	0.00	0.00	2	1	0.770	51	51	52	3.60	2.70	1	1	0.122
15	15	16	45.50	30.00	2	1	0.143	52	9	53	4.35	3.50	6	1	0.319
16	16	17	60.00	35.00	2	1	0.272	53	53	54	26.40	19.00	6	1	0.373
17	17	18	60.00	35.00	2	1	0.003	54	54	55	24.00	17.20	6	1	0.522
18	18	19	0.00	0.00	2	1	0.238	55	55	56	0.00	0.00	6	1	0.516
19	19	20	1.00	0.60	2	1	0.153	56	56	57	0.00	0.00	6	1	2.918
20	20	21	114.00	81.00	1	1	0.126	57	57	58	0.00	0.00	6	1	1.438
21	21	22	5.30	3.50	1	1	0.005	58	58	59	100.00	72.00	6	1	0.558
22	22	23	0.00	0.00	1	1	0.059	59	59	60	0.00	0.00	5	1	0.568
23	23	24	28.00	20.00	1	1	0.127	60	60	61	1244.00	888.00	5	1	0.747
24	24	25	0.00	0.00	1	1	0.275	61	61	62	32.00	23.00	1	1	0.036
25	25	26	14.00	10.00	1	1	0.114	62	62	63	0.00	0.00	1	1	0.053
26	26	27	14.00	10.00	1	1	0.064	63	63	64	227.00	162.00	1	1	0.261
27	3	28	26.00	18.60	1	1	0.002	64	64	65	59.00	42.00	1	1	0.383
28	28	29	26.00	18.60	1	1	0.024	65	11	66	18.00	13.00	1	1	0.074
29	29	30	0.00	0.00	1	1	0.146	66	66	67	18.00	13.00	1	1	0.002
30	30	31	0.00	0.00	1	1	0.026	67	12	68	28.00	20.00	1	1	0.272
31	31	32	0.00	0.00	1	1	0.129	68	68	69	28.00	20.00	1	1	0.002
32	32	33	14.00	10.00	1	1	0.309	69	11	43			1	0	0.184
33	33	34	19.50	14.00	1	1	0.628	70	13	21			1	0	0.184
34	34	35	6.00	4.00	1	1	0.542	71	15	46			1	0	0.368
35	3	36	26.00	18.55	1	1	0.002	72	50	59			1	0	0.736
36	36	37	26.00	18.55	1	1	0.024	73	27	65			1	0	0.368
37	37	38	0.00	0.00	1	1	0.039								

Table A3. Initial electrical data for the 83-bus test system.

Branch	Branch		P	Q	Conductor	Operation	Length	Branch	Branch		P	Q	Conductor	Operation	Length
	From	To	[kW]	[kVAr]	Type	State	[km]		From	To	[kW]	[kVAr]	Type	State	[km]
1	0	1	0.0	0.0	14	1	0.88646	49	48	49	0.0	0.0	13	1	0.23862
2	1	2	100.0	50.0	14	1	0.95577	50	49	50	200.0	160.0	13	1	0.14317
3	2	3	300.0	200.0	14	1	1.07524	51	50	51	800.0	600.0	13	1	0.28634
4	3	4	350.0	250.0	14	1	0.41815	52	51	52	500.0	300.0	13	1	0.14317
5	4	5	220.0	100.0	14	1	0.65577	53	52	53	500.0	350.0	13	1	0.28634
6	5	6	1100.0	800.0	12	1	0.23013	54	53	54	500.0	300.0	13	1	0.03814
7	6	7	400.0	320.0	5	1	0.98960	55	54	55	200.0	80.0	13	1	0.04820
8	7	8	300.0	200.0	1	1	0.38560	56	0	56	0.0	0.0	5	1	0.33377
9	7	9	300.0	230.0	1	1	0.86750	57	56	57	30.0	20.0	5	1	0.79043
10	7	10	300.0	260.0	1	1	0.38560	58	57	58	600.0	420.0	5	1	0.07712
11	0	11	0.9	0.0	13	1	0.28634	59	58	59	0.0	0.0	5	1	0.02948
12	11	12	1200.0	800.0	13	1	1.24080	60	59	60	20.0	10.0	5	1	0.02860
13	12	13	800.0	600.0	5	1	0.01907	61	60	61	20.0	10.0	5	1	0.01907
14	12	14	700.0	500.0	13	1	0.05721	62	61	62	200.0	130.0	5	1	0.07627
15	0	15	0.0	0.0	17	1	0.61497	63	62	63	300.0	240.0	5	1	0.08675
16	15	16	300.0	150.0	17	1	0.28416	64	63	64	300.0	200.0	5	1	0.00894
17	16	17	500.0	350.0	16	1	0.23593	65	0	65	0.0	0.0	15	1	0.21951
18	17	18	700.0	400.0	16	1	0.70779	66	65	66	50.0	30.0	15	1	0.76920
19	18	19	1200.0	1000.0	7	1	0.08609	67	66	67	0.0	0.0	15	1	0.54878
20	19	20	300.0	300.0	7	1	0.12394	68	67	68	400.0	360.0	15	1	0.98780
21	20	21	400.0	350.0	1	1	0.08675	69	68	69	0.0	0.0	9	1	0.12653
22	21	22	50.0	20.0	1	1	0.05784	70	69	70	0.0	0.0	9	1	0.18979

Table A3. *Cont.*

Branch	Branch		P	Q	Conductor	Operation	Length	Branch	Branch		P	Q	Conductor	Operation	Length
	From	To	[kW]	[kVAr]	Type	State	[km]		From	To	[kW]	[kVAr]	Type	State	[km]
23	21	23	50.0	20.0	1	1	0.07230	71	70	71	2000.0	1500.0	9	1	0.14762
24	23	24	50.0	10.0	1	1	0.04821	72	71	72	200.0	150.0	9	1	0.00964
25	0	25	50.0	30.0	7	1	0.12421	73	0	73	0.0	0.0	5	1	0.47682
26	25	26	100.0	60.0	7	1	0.22957	74	73	74	0.0	0.0	5	1	0.04768
27	26	27	100.0	70.0	7	1	0.54524	75	74	75	1200.0	950.0	5	1	0.08344
28	27	28	1800.0	1300.0	7	1	0.10646	76	75	76	300.0	180.0	5	1	0.07152
29	28	29	200.0	120.0	6	1	0.04820	77	0	77	0.0	0.0	17	1	1.36171
30	0	30	0.0	0.0	17	1	1.06562	78	77	78	400.0	360.0	17	1	0.70282
31	30	31	1800.0	1600.0	17	1	0.71041	79	78	79	2000.0	1300.0	17	1	0.26356
32	31	32	200.0	150.0	17	1	0.24041	80	79	80	200.0	140.0	7	1	0.14370
33	32	33	200.0	100.0	6	1	0.04808	81	80	81	500.0	360.0	7	1	0.09534
34	33	34	800.0	600.0	6	1	0.18681	82	81	82	100.0	30.0	7	1	0.03374
35	34	35	100.0	60.0	6	1	0.01928	83	82	83	400.0	360.0	7	1	0.11567
36	35	36	100.0	60.0	6	1	0.18315	84	5	55	0.0	0.0	13	0	0.47723
37	36	37	20.0	10.0	6	1	0.01446	85	7	60	0.0	0.0	5	0	0.19279
38	37	38	20.0	10.0	6	1	0.01446	86	11	43	0.0	0.0	13	0	0.47723
39	38	39	20.0	10.0	6	1	0.02892	87	12	72	0.0	0.0	13	0	1.24080
40	39	40	20.0	10.0	6	1	0.07712	88	13	76	0.0	0.0	5	0	0.67476
41	38	41	200.0	160.0	6	1	0.07230	89	14	18	0.0	0.0	16	0	2.41828
42	41	42	50.0	30.0	6	1	0.07712	90	16	26	0.0	0.0	20	0	0.74980
43	0	43	0.0	0.0	2	1	0.03537	91	20	83	0.0	0.0	7	0	0.17218
44	43	44	30.0	20.0	2	1	0.02860	92	28	32	0.0	0.0	17	0	0.28416
45	44	45	800.0	700.0	2	1	0.09534	93	29	39	0.0	0.0	6	0	0.14425
46	45	46	200.0	150.0	2	1	0.08675	94	34	46	0.0	0.0	6	0	0.04808
47	0	47	0.0	0.0	13	1	0.88525	95	40	42	0.0	0.0	6	0	0.36062
48	47	48	0.0	0.0	13	1	0.23862	96	53	64	0.0	0.0	5	0	0.05784

References

1. Swaminathan, D.; Rajagopalan, A.; Montoya, O.D.; Arul, S.; Grisales-Noreña, L.F. Distribution Network Reconfiguration Based on Hybrid Golden Flower Algorithm for Smart Cities Evolution. *Energies* **2023**, *16*, 2454. [CrossRef]
2. Grisales-Noreña, L.F.; Rosales-Muñoz, A.A.; Montoya, O.D. An Effective Power Dispatch of Photovoltaic Generators in DC Networks via the Antlion Optimizer. *Energies* **2023**, *16*, 1350. [CrossRef]
3. Wang, Z.; Liu, H.; Yu, D.; Wang, X.; Song, H. A practical approach to the conductor size selection in planning radial distribution systems. *IEEE Trans. Power Deliv.* **2000**, *15*, 350–354. [CrossRef]
4. Sivanagaraju, S.; Sreenivasulu, N.; Vijayakumar, M.; Ramana, T. Optimal conductor selection for radial distribution systems. *Electr. Power Syst. Res.* **2002**, *63*, 95–103. [CrossRef]
5. Mandal, S.; Pahwa, A. Optimal selection of conductors for distribution feeders. *IEEE Trans. Power Syst.* **2002**, *17*, 192–197. [CrossRef]
6. Kaur, D.; Sharma, J. Optimal conductor sizing in radial distribution systems planning. *Int. J. Electr. Power Energy Syst.* **2008**, *30*, 261–271. [CrossRef]
7. Thenepalle, M. A Comparative Study on Optimal Conductor Selection for Radial Distribution Network using Conventional and Genetic Algorithm Approach. *Int. J. Comput. Appl.* **2011**, *17*, 6–13. [CrossRef]
8. Abul'Wafa, A.R. Multi-conductor feeder design for radial distribution networks. *Electr. Power Syst. Res.* **2016**, *140*, 184–192. [CrossRef]
9. Ali, H.; Ullah, S.; Sami, I.; Ahmad, N.; Khan, F. Economic Loss Minimization of a Distribution Feeder and Selection of Optimum Conductor for Voltage Profile Improvement. In Proceedings of the 2018 International Conference on Power Generation Systems and Renewable Energy Technologies (PGSRET), Islamabad, Pakistan, 10–12 September 2018; pp. 1–6. [CrossRef]
10. Mozaffari, L.M.; Hassan, J.; Mohammad, L. Optimal Conductor Selection in Radial Distribution Systems for Productivity Improvement Using Genetic Algorithm. *Iraqi J. Electr. Electron. Eng.* **2013**, *9*, 29–35. [CrossRef]
11. Zhao, Z.; Mutale, J. Optimal Conductor Size Selection in Distribution Networks with High Penetration of Distributed Generation Using Adaptive Genetic Algorithm. *Energies* **2019**, *12*, 2065. [CrossRef]
12. Mendoza, F.; Requena, D.; Bemal-agustin, J.L.; Dominguez-navarro, J.A. Optimal Conductor Size Selection in Radial Power Distribution Systems Using Evolutionary Strategies. In Proceedings of the 2006 IEEE/PES Transmission & Distribution Conference and Exposition: Latin America, Caracas, Venezuela, 15–18 August 2006; pp. 1–5. [CrossRef]

13. Samal, P.; Mohanty, S.; Ganguly, S. Simultaneous capacitor allocation and conductor sizing in unbalanced radial distribution systems using differential evolution algorithm. In Proceedings of the 2016 National Power Systems Conference (NPSC), Bhubaneswar, India, 19–21 December 2016; pp. 1–6. [CrossRef]
14. Farahani, V.; Sadeghi, S.H.H.; Askarian Abyaneh, H.; Agah, S.M.M.; Mazlumi, K. Energy Loss Reduction by Conductor Replacement and Capacitor Placement in Distribution Systems. *IEEE Trans. Power Syst.* **2013**, *28*, 2077–2085. [CrossRef]
15. Mozaffari Legha, M. Combination of Optimal Conductor Selection and Capacitor Placement in Radial Distribution Systems Using PSO Method. *Iraqi J. Electr. Electron. Eng.* **2014**, *10*, 33–41. [CrossRef]
16. Kumari, M.; Ranjan, R. Economical Selection of Conductor in Radial Distribution System using PSO. *J. Inst. Eng. (India) Ser. B* **2022**, *103*, 1105–1114. [CrossRef]
17. Khalil, T.M.; Gorpinich, A.V. Optimal conductor selection and capacitor placement for loss reduction of radial distribution systems by selective particle swarm optimization. In Proceedings of the 2012 Seventh International Conference on Computer Engineering & Systems (ICCES), Cairo, Egypt, 27–29 November 2012; pp. 215–220. [CrossRef]
18. Manikandan, S.; Sasitharan, S.; Rao, J.V.; Moorthy, V. Analysis of optimal conductor selection for radial distribution systems using DPSO. In Proceedings of the 2016 3rd International Conference on Electrical Energy Systems (ICEES), Chennai, India, 17–19 March 2016; pp. 96–101. [CrossRef]
19. Ismael, S.M.; Abdel Aleem, S.H.E.; Abdelaziz, A.Y.; Zobaa, A.F. Practical Considerations for Optimal Conductor Reinforcement and Hosting CapaEconomic Loss Minimization of a Distribution Feeder and Selection of Optimum 435 Conductor for Voltage Profile Improvement. Enhancement in Radial Distribution Systems. *IEEE Access* **2018**, *6*, 27268–27277. [CrossRef]
20. Srinivas, R.R.; Satish, K.; Narasimham, S.V.L. Optimal Conductor Size Selection in Distribution Systems Using the Harmony Search Algorithm with a Differential Operator. *Electr. Power Components Syst.* **2011**, *40*, 41–56. [CrossRef]
21. Abdelaziz, A.Y.; Fathy, A. A novel approach based on crow search algorithm for optimal selection of conductor size in radial distribution networks. *Eng. Sci. Technol. Int. J.* **2017**, *20*, 391–402. [CrossRef]
22. Ismael, S.M.; Aleem, S.H.E.A.; Abdelaziz, A.Y. Optimal selection of conductors in Egyptian radial distribution systems using sine-cosine optimization algorithm. In Proceedings of the 2017 Nineteenth International Middle East Power Systems Conference (MEPCON), Cairo, Egypt, 19–21 December 2017; pp. 103–107. [CrossRef]
23. Montoya, O.D.; Grajales, A.; Hincapié, R.A. Selección òptima de conductores en sistemas de distribución empleando el algoritmo búsqueda tabú. *Ingeniare Rev. Chil. De Ing.* **2018**, *26*, 283–295. [CrossRef]
24. Nivia-Torres, D.J.; Salazar-Alarcon, G.A.; Montoya, O.D. Selección óptima de conductores en redes de distribución trifásicas utilizando el algoritmo metaheurístico de Newton. *Ingeniería* **2022**, *27*, 334–354. [CrossRef]
25. Franco, J.F.; Rider, M.J.; Lavorato, M.; Romero, R. Optimal Conductor Size Selection and Reconductoring in Radial Distribution Systems Using a Mixed-Integer LP Approach. *IEEE Trans. Power Syst.* **2013**, *28*, 10–20. [CrossRef]
26. Montoya, O.D.; Garces, A.; Castro, C.A. Optimal Conductor Size Selection in Radial Distribution Networks Using a Mixed-Integer Non-Linear Programming Formulation. *IEEE Lat. Am. Trans.* **2018**, *16*, 2213–2220. [CrossRef]
27. Farrag, M.A.; Khalil, A.H.; Omran, S. Optimal conductor selection and capacitor placement in radial distribution system using nonlinear AC load flow equations and dynamic load model. *Int. Trans. Electr. Energy Syst.* **2020**, *30*, e12316. [CrossRef]
28. Montoya, O.D.; Gil-González, W.; Grisales-Noreña, L.F. On the mathematical modeling for optimal selecting of calibers of conductors in DC radial distribution networks: A MINLP approach. *Electr. Power Syst. Res.* **2021**, *194*, 107072. [CrossRef]
29. Gallego Pareja, L.A.; López-Lezama, J.M.; Gómez Carmona, O. A Mixed-Integer Linear Programming Model for the Simultaneous Optimal Distribution Network Reconfiguration and Optimal Placement of Distributed Generation. *Energies* **2022**, *15*, 3063. [CrossRef]
30. Shirmohammadi, D.; Hong, H. Reconfiguration of electric distribution networks for resistive line losses reduction. *IEEE Trans. Power Deliv.* **1989**, *4*, 1492–1498. [CrossRef]
31. Ahmadi, H.; Martí, J.R. Mathematical representation of radiality constraint in distribution system reconfiguration problem. *Int. J. Electr. Power Energy Syst.* **2015**, *64*, 293–299. [CrossRef]
32. Gomes, F.; Carneiro, S.; Pereira, J.; Vinagre, M.; Garcia, P.; De Araujo, L. A New Distribution System Reconfiguration Approach Using Optimum Power Flow and Sensitivity Analysis for Loss Reduction. *IEEE Trans. Power Syst.* **2006**, *21*, 1616–1623. [CrossRef]
33. Sivanagaraju, S.; Rao, J.V.; Raju, P.S. Discrete Particle Swarm Optimization to Network Reconfiguration for Loss Reduction and Load Balancing. *Electr. Power Components Syst.* **2008**, *36*, 513–524. [CrossRef]
34. Abdelaziz, A.; Mohammed, F.; Mekhamer, S.; Badr, M. Distribution Systems Reconfiguration using a modified particle swarm optimization algorithm. *Electr. Power Syst. Res.* **2009**, *79*, 1521–1530. [CrossRef]
35. Yang, M.; Li, J.; Li, J.; Yuan, X.; Xu, J. Reconfiguration Strategy for DC Distribution Network Fault Recovery Based on Hybrid Particle Swarm Optimization. *Energies* **2021**, *14*, 7145. [CrossRef]
36. Zhu, J. Optimal reconfiguration of electrical distribution network using the refined genetic algorithm. *Electr. Power Syst. Res.* **2002**, *62*, 37–42. [CrossRef]
37. He, M.; Ma, C.; Duan, Q.; Ni, S.; Deng, W.; Liu, X.; Li, Z.; Chen, Y.; Shi, Y. Active Distribution Network Reconfiguration Method Based on Photovoltaic Generation Prediction. In Proceedings of the 2022 IEEE International Conference on Electrical Engineering, Big Data and Algorithms (EEBDA), Changchun, China, 25–27 February 2022; pp. 82–87. [CrossRef]
38. Wang, C.; Gao, Y. Determination of Power Distribution Network Configuration Using Non-Revisiting Genetic Algorithm. *IEEE Trans. Power Syst.* **2013**, *28*, 3638–3648. [CrossRef]

39. Eldurssi, A.M.; O'Connell, R.M. A Fast Nondominated Sorting Guided Genetic Algorithm for Multi-Objective Power Distribution System Reconfiguration Problem. *IEEE Trans. Power Syst.* **2015**, *30*, 593–601. [CrossRef]
40. Guimarães, M.A.; Castro, C.A.; Romero, R. Distribution systems operation optimization through reconfiguration and capacitor allocation by a dedicated genetic algorithm. *IET Gener. Transm. Distrib.* **2010**, *4*, 1213. [CrossRef]
41. Guamán, A.; Valenzuela, A. Distribution Network Reconfiguration Applied to Multiple Faulty Branches Based on Spanning Tree and Genetic Algorithms. *Energies* **2021**, *14*, 6699. [CrossRef]
42. Amin, A.; Muhammad, M.; Mokhlis, H.; Franco, J.; Naidu, K.; Coo, L. Enhancement of Simultaneous Network Reconfiguration and DG Sizing via Hamming dataset approach and Firefly Algorithm. *IET Gener. Transm. Distrib.* **2019**, *13*, 5071–5082. [CrossRef]
43. Gerez, C.; Silva, L.I.; Belati, E.A.; Sguarezi Filho, A.J.; Costa, E.C.M. Distribution Network Reconfiguration Using Selective Firefly Algorithm and a Load Flow Analysis Criterion for Reducing the Search Space. *IEEE Access* **2019**, *7*, 67874–67888. [CrossRef]
44. Srinivasa Rao, R.; Narasimham, S.V.L.; Ramalinga Raju, M.; Srinivasa Rao, A. Optimal Network Reconfiguration of Large-Scale Distribution System Using Harmony Search Algorithm. *IEEE Trans. Power Syst.* **2011**, *26*, 1080–1088. [CrossRef]
45. Santos, M.V.D.; Brigatto, G.A.; Garcés, L.P. Methodology of solution for the distribution network reconfiguration problem based on improved harmony search algorithm. *IET Gener. Transm. Distrib.* **2020**, *14*, 6526–6533. [CrossRef]
46. Zhang, D.; Fu, Z.; Zhang, L. An improved TS algorithm for loss-minimum reconfiguration in large-scale distribution systems. *Electr. Power Syst. Res.* **2007**, *77*, 685–694. [CrossRef]
47. Abdelaziz, A.; Mohamed, F.; Mekhamer, S.; Badr, M. Distribution system reconfiguration using a modified Tabu Search algorithm. *Electr. Power Syst. Res.* **2010**, *80*, 943–953. [CrossRef]
48. Liu, N.; Li, C.; Chen, L.; Wang, J. Hybrid Data-Driven and Model-Based Distribution Network Reconfiguration With Lossless Model Reduction. *IEEE Trans. Ind. Inform.* **2022**, *18*, 2943–2954. [CrossRef]
49. Zhang, Z.; Du, W.; Lu, Y.; Xu, G.; Zhao, Y. Two-Stage Robust Distribution Network Reconfiguration Against Failures of Lines and Renewable Generations. *IEEE Access* **2022**, *10*, 108614–108624. [CrossRef]
50. Gautam, M.; Bhusal, N.; Benidris, M. Deep Q-Learning-based Distribution Network Reconfiguration for Reliability Improvement. In Proceedings of the 2022 IEEE/PES Transmission and Distribution Conference and Exposition (T&D), New Orleans, LA, USA, 25–28 April 2022; pp. 1–5. [CrossRef]
51. Dai, B. Multi-objective Optimization Model of Distribution Network Reconfiguration Considering Soft Open Point. In Proceedings of the 2022 China International Conference on Electricity Distribution (CICED), Changsha, China, 7–8 September 2022; pp. 468–472. . [CrossRef]
52. Wen, J.; Qu, X.; Huang, Y.; Lin, S. A Reconfiguration Method of Distribution Network Considering Time Variations for Load and Renewable Distributed Generation. In Proceedings of the 2022 7th Asia Conference on Power and Electrical Engineering (ACPEE), Hangzhou, China, 15–17 April 2022; pp. 544–549. [CrossRef]
53. Razavi, S.M.; Momeni, H.R.; Haghifam, M.R.; Bolouki, S. Multi-Objective Optimization of Distribution Networks via Daily Reconfiguration. *IEEE Trans. Power Deliv.* **2022**, *37*, 775–785. [CrossRef]
54. Mahdavi, M.; Alhelou, H.H.; Bagheri, A.; Djokic, S.Z.; Ramos, R.A.V. A Comprehensive Review of Metaheuristic Methods for the Reconfiguration of Electric Power Distribution Systems and Comparison With a Novel Approach Based on Efficient Genetic Algorithm. *IEEE Access* **2021**, *9*, 122872–122906. [CrossRef]
55. Chen, F.; Lu, H.; Tong, Z.; Wu, J.; Lu, C. Research on Path Connectivity Optimization Model for Active Distribution Network Reconfiguration. In Proceedings of the 2022 5th International Conference on Renewable Energy and Power Engineering (REPE), Beijing, China, 28–30 September 2022; pp. 233–236. [CrossRef]
56. Tavakoli Ghazi Jahani, M.; Nazarian, P.; Safari, A.; Haghifam, M. Multi-objective optimization model for optimal reconfiguration of distribution networks with demand response services. *Sustain. Cities Soc.* **2019**, *47*, 101514. [CrossRef]
57. Haghighat, H.; Zeng, B. Distribution System Reconfiguration Under Uncertain Load and Renewable Generation. *IEEE Trans. Power Syst.* **2016**, *31*, 2666–2675. [CrossRef]
58. Gallego, L.A.; López-Lezama, J.M.; Carmona, O.G. A Mixed-Integer Linear Programming Model for Simultaneous Optimal Reconfiguration and Optimal Placement of Capacitor Banks in Distribution Networks. *IEEE Access* **2022**, *10*, 52655–52673. [CrossRef]
59. Gallego Pareja, L.A.; López-Lezama, J.M.; Gómez Carmona, O. A MILP Model for Optimal Conductor Selection and Capacitor Banks Placement in Primary Distribution Systems. *Energies* **2023**, *16*, 4340. [CrossRef]